JTTEE5 15:97-105
DOI: 10.1361/105996306X92668
1059-9630/$19.00 © ASM International

Particle Characterization and Splat Formation of Plasma Sprayed Zirconia

Li Li, Anirudha Vaidya, Sanjay Sampath, Hongbing Xiong, and Lili Zheng

(Submitted January 20, 2005; in revised form July 13, 2005)

A process map study has been carried out to examine the role of process variables on the properties of deposit formed in thermal spray. In the past, droplet size, temperature, and velocity have been widely used to interpret the status of in-flight particles. However, the limitation of those parameters on describing the molten fraction of refractory ceramics limits these parameters' qualifications and validation on examining the causes of the resulting deposit. In this study, a group parameter, melting index, is used to interpret the molten state of particles, which also reflects the thermal energy of the particles. The kinetic energy and fluidity of particles are characterized through their Reynolds number. Splat morphological features such as flattening and fragmentation are characterized against the group parameters. Deposition rate test confirms the significance of the concept of melting index. It is highlighted in this paper that particle group parameters, i.e., melting index and Reynolds number describe the particle in-flight status very well and can be used to predict the deposit behaviors.

Keywords deposition rate, melting index, Reynolds number, splat morphology

1. Introduction

Plasma spray is an established coating technology, in which powder particles injected into plasma jet are quickly melted and propelled onto substrate. The molten or semimolten droplets impinge on a substrate and rapidly solidify to form single splats. The coating is built up by piling up the layers of splats. Quality and functionality of the coating are dependent upon the nature of sprayed materials as well as the microstructure of the coating. It has been proven that the microstructure of the coating is attributed not only to the nature of the coating material, but also to the process conditions. Because the coating is built up through overlapping splats, the spreading and solidification of splats on both substrate and previous deposit are essential to determine the consequential coating microstructure.

Splat formation is sensitive to the status of droplet before impact, the nature of substrate material, and the substrate surface conditions. This paper will focus mainly on the effect of particle in-flight conditions. Particle motion and heating is a well-researched area. The effects of particle size, velocity, and temperature on splat morphology have been studied extensively, both numerically and experimentally (Ref 1-6). It was found that the splat flattening ratio increase when the particle velocity and temperature increase and the fragmentation of the splat increase with the increase of the particle kinetic energy. Based on macroscopic mechanical energy balance, Madejski model (Ref 7) and a modified version (Ref 8) have been developed to correlate the particle Reynolds number (*Re*) and temperature with the flattening ratio and solidification of a disk-like splat. Melting behavior of an in-flight particle has also drawn a significant attention (Ref 9-11). As shown in Fig. 1, partially melted or unmelted particles are observed in many cases, however none of the above research evaluated the effect of molten fraction of refractory particles on their resulting deposit properties, not to mention to quantify this effect. To better interpret the refractory particle's in-flight status, a group parameter, melting index (*MI*), was introduced by Vaidya et al. (Ref 12) based on experimentally available parameters such as in-flight particle surface temperature, velocity, and the size of the particles, which can be monitored by an on-line diagnostic systems. Melting index was further defined by Zhang et al. (Ref 13). This parameter, at the first time, serves as an indicator of the melting behavior of the in-flight particles. Although theoretically it is still an enigma how the melting fraction affects the splat morphology, experimental results show that partially melted particles does exhibit apparent different splat morphologies as compared with a fully molten one. Also, the presence of partially melted particles may result in a lower efficiency of deposition, and a higher porosity, and a different microstructure of coatings.

In this paper, dedicated experiments have been carried out to evaluate the role of the group parameters of process, i.e., *MI* and *Re,* on partially stabilized zirconia deposit due to its extensive usage in the aerospace industry. These parameters are used to interpret the status of in-flight particles and account for the resulting deposit properties. Data have been collected on the size distribution of powder feedstock, in-flight temperature, velocity, and dimensions of particles, consequentially *Re* and *MI* can be calculated. Deposit properties, such as splat flattening ratio, fragmentation degree, and deposition rate have been measured to correlate to particles in flight conditions.

Li Li, Anirudha Vaidya, and **Sanjay Sampath,** Department of Materials Science and Engineering, State University of New York at Stony Brook, Stony Brook, NY 11794; and **Hongbing Xiong** and **Lili Zheng,** Department of Mechanical Engineering, State University of New York at Stony Brook, Stony Brook, NY 11794. Contact e-mail: lili@engineering.ucsb.edu.

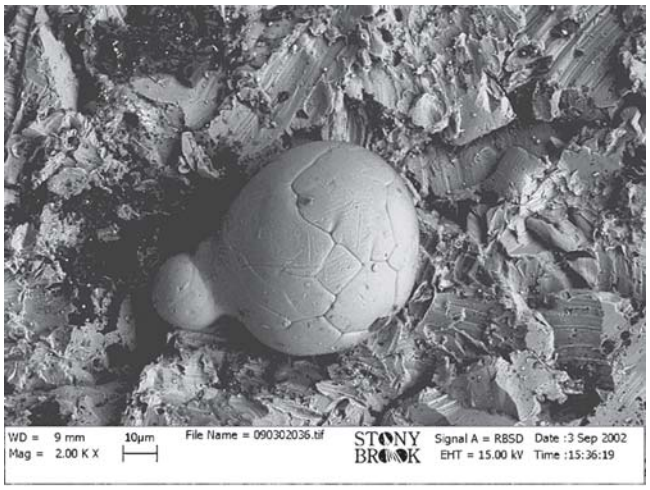

(a)

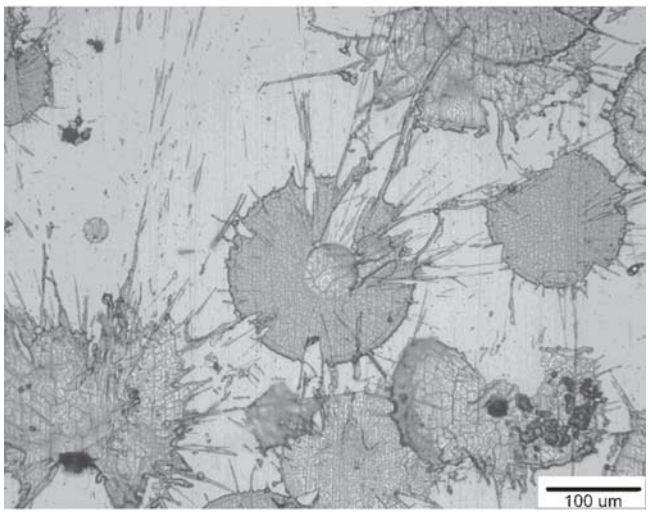

(b)

Fig. 1 (a) Unmelted nickel particle and (b) zirconia splat with unmelted core

2. Mathematical Equations for Particle Conditions Characterization

In this study, individual parameters, particle size (d), surface temperature (T_s), velocity (v), are converted to group parameters, Reynolds number (Re), and melting index (MI). For Reynolds number, $Re = \rho v d/\mu$, where ρ and μ are particle density and dynamic viscosity, respectively; the melting index is defined as the ratio of the particle dwelling time to the time required to melt the particle. A higher MI indicates a better molten status. Low MI reflects partial or unmelted conditions. For MI calculation (Ref 13):

$$MI = A\,\frac{24k}{\rho h_{fg}}\,\frac{1}{1+4/Bi}\cdot\frac{(T_s - T_m)\cdot\Delta t_{fly}}{d^2} \qquad \text{(Eq 1)}$$

where MI is melting index; and A is a dimensionless factor defined as $(T_f - T_m)/(T_s - T_m)$, where T_f is flame temperature, T_s is particle surface temperature, and T_m is particle melting point; k is thermal conductivity of liquid, h_{fg} is latent heat; Bi is Biot number defined as hd/k, where d is particle diameter, h is heat transfer coefficient; and Δt_{fly} is particle dwelling time, estimated as $2L/v$, where L is stand off distance and v is particle velocity.

Because T_f is not available directly from the measurement, factor A cannot be resolved precisely so far. In this paper, A is assumed to be unity, and the heat transfer coefficient h is assumed constant for all calculations. Thermophysical properties used in the calculation are summarized in Table 1.

3. Experimental Process

Partially stabilized zirconia AE7592 from Sulzer-Metco (Westbury, NY) with a mean size of 35 µm was used as the feedstock. The powder size distribution was measured by particle characterization analyzer from Beckman Coulter (Fullerton, CA). The in-flight particle size (d), surface temperature (T_s) and velocity (v) were monitored by Tecnar DPV 2000 (St. Bruno, Canada) diagnostic system (Ref 14). Two sets of torches have been used in this study to ensure the effect of group parameters defined as independent upon the hardware. Setup 1 used a PTF 4 MB direct current plasma gun with a 7 mm nozzle, controlled through the PT A 2000 console. A PT twin-system 10 dual powder feeder with an external injection port 1.5 mm in diameter was used as the feeding system. Splats were collected at a spray distance of 120 mm in this setup by rotating the substrate. Setup 2 used SG-100 torch (Miller Thermal) with a 175 nozzle. The torch was mounted on a six-axis Fanuc GMF Robotic S-400 robot. A Miller Thermal #1270 powder feeder was used for powder feeding. The powder injection was internal to the nozzle with an opening of 2 mm diameter. Splats were collected at positions of 60, 80, 100, and 120 mm from the nozzle, respectively, by rapidly moving the torch across the substrate. Tables 2 and 3 list the spray parameters over which the particle size, velocity, and temperature were measured.

In both cases, droplets were deposited on mirror polished type 304 stainless steel substrates (roughness $Ra = 0.05$ µm) at room temperature. The sample sizes were 2 × 1 in. for setup 1 and 1 × 1 in. for setup 2. A large number of splats (70 splats for setup 1, 30 splats for setup 2 at each spray distance) were scanned by means of Zygo New Viewer 200 (Middlefield, CT), a scanning white light interferometry (SWLI) (Ref 15). This microscopy has a horizontal resolution similar to that obtained by optical microscopy and a vertical resolution of 1 nm. The splat parameters measured from SWLI are volume (V), diameter (D), and thickness (b). UTHSCSA Image Tool (Wohlen, Switzerland) was used to measure the perimeter (P) of a single splat as well as the area (A). Based on the above measurements, splat flattening ratio D/d and fragmentation degree $P^2/(4\pi A)$ could be resolved. The value of fragmentation degree ranges from 1 to infinity. It describes how far away from a perfect disk shape the splat morphology is; the larger the number, the higher the fragmentation.

The best way to correlate the splat flattening ratio and fragmentation degree to the process parameter is to achieve a "one-to-one" correspondence between a particle and its resulting splat. However, it is nearly impossible to reach this in the current setup. One way to make it close is to average the process parameters of a group of particles with the same volume range as it is measured from single splats. In other words, if it is assumed that

particles have spherical shapes and there is no volume loss after impact, a splat with a volume of V μm^3 should stem from a particle droplet of a size about $(6V/\pi)^{1/3}$. In this way, those splats collected on the substrate all found their "parent particles."

In setup 2, along the spray distance the weight differences of the substrates before and after spraying were measured, in addition to the splat morphology characterization. The increasing weight was then normalized by the dimensions of the sample coupons. The deposition rate, defined as the gain in weight per unit length, is compared against the average particle temperature, velocity, and average melting index data from in-flight diagnostics.

Table 1 Thermophysical properties of YSZ used in the calculations

k, W m^{-1} K^{-1}	ρ, kg m^{-3}	T_m, K	h_{fg}, J kg^{-1}	h, W m^{-2} K^{-1}	μ, kg m^{-1} s^{-1}
2.32	5.7×10^3	2.95×10^3	7.07×10^5	1.5×10^3	3.7×10^{-2}

Table 2 Spray parameters for PT F4 torch in setup 1

Current, A	Voltage, V	Ar, SLM	H_2, SLM	Carrier gas, SLM	Feeding rate, rpm	Spray distance, mm
600	69	32	8	3	1.5	120

Table 3 Spray parameters for SG-100 torch in setup 2

Current, A	Voltage, V	Ar, SLM	He, SLM	Carrier gas, SLM	Feeding rate, rpm	Spray distance, mm
850	39	39	21	4.5	1.5	60-120

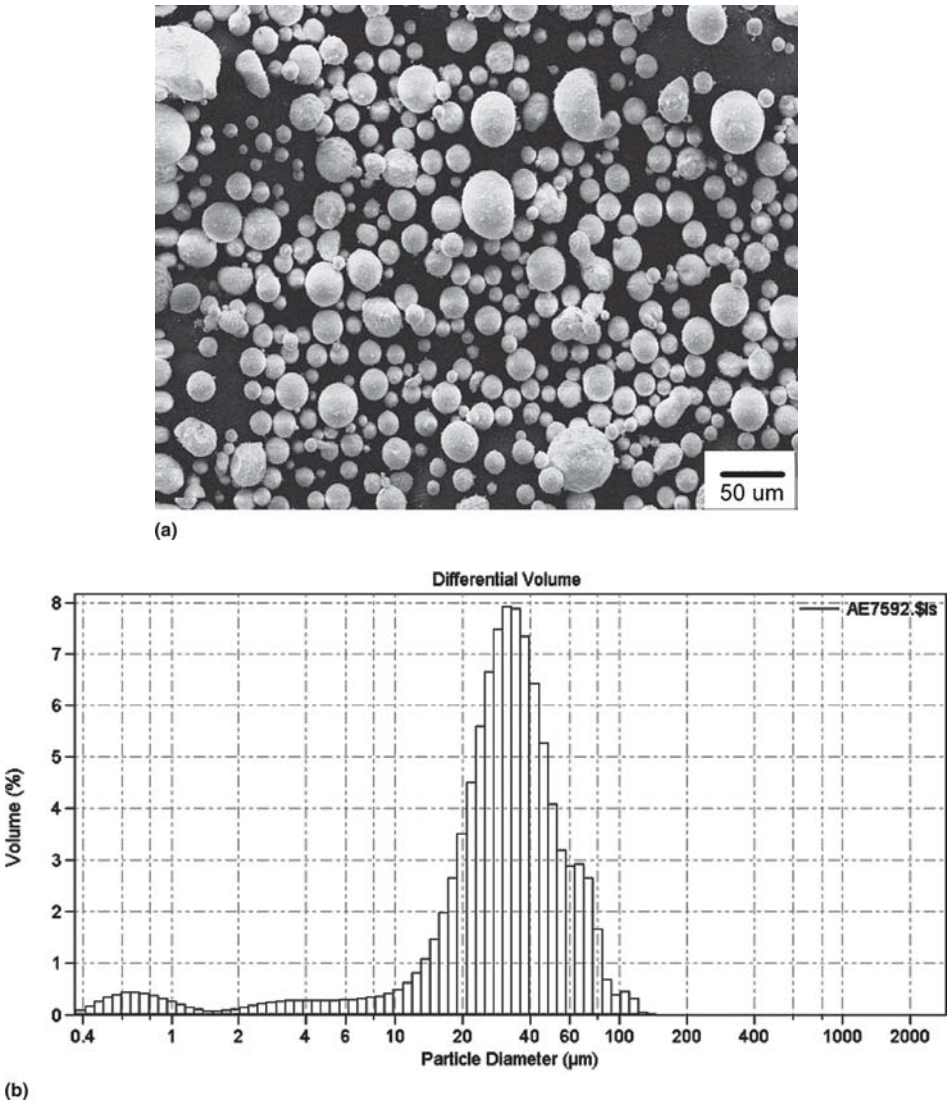

Fig. 2 (a) Morphology of partially stabilized zirconia (PSZ) (AE7592) powder and (b) powder size distribution

4. Results and Discussion

4.1 In-Flight Diagnostics and Particle Characterization

Figure 2(a) illustrates the electron microscopy of the feedstock used in this study; AE 7592 is a plasma densified HOSP powder. Obviously, this commercial powder has a large size distribution, as shown in Fig. 2(b). Therefore a large distribution of in-flight particle size would be expected; a large distribution would also be expected for the surface temperature and particle velocity due to the size effect and the difference of the flight trajectories. Figure 3 plots the statistic data of d, T_s, and v from the diagnostic recording during the experiment using setup 1, based on which the group parameters, particle Re, and melting index were calculated (Fig. 4). The large distribution of MI and Re suggests a significant diversity of the splat morphologies.

4.2 Effect of Process Parameters on Splat Morphology

The relationship of particle flattening ratio ξ_m and Re is plotted in Fig. 5. The experimental data are also compared with the modeling prediction, $\xi_m = 1.18\ Re^{0.2}$ (Ref 8). The model is developed using high-order velocity distribution and accounting for the adhesion between molten droplet and substrate. The outcome confirms the effects of particle Re on the splat flattening behavior. No apparent relationship has been found between flattening ratio and MI during this study. However, it is found that the fragmentation degree is a function of both Re and MI. Random data of fragmentation degree (Z axis), Re (X axis), and MI (Y axis) in the worksheet were converted into a regular grid (a matrix) through a correlation method or Kriging method (Ref 16). A three-dimensional map (Fig. 6) is then generated based on the matrix. It is demonstrated from Fig. 6 that the splat fragmentation degree depends primarily on particle Re, whereas in the same range of Re, particles with larger MI tend to fragment less.

The same method has been used to analyze the data collected from the four spray distances of 60, 80, 100, and 120 mm (in setup 2). The fragmentation map is plotted in Fig. 7 based on the data from all splats collected at each spray distance. Once again, it is highlighted that particles with higher values of Re and lower values of MI prefer to form more fragmented splats. However, the map is not ideally smooth. There are two possible reasons accounting for this. First, relatively larger error of in-flight diagnostic may arise on small size particles due to their less thermal radiations. Second, although the same type of substrate is used, local surface conditions (roughness and contamination) are not exactly the same, and the substrate conditions are quite significant in determining the splat morphology (Ref 17-19). For the same reason, the results from Fig. 6 and 7 are not exactly comparable due to noticeable preheating of the substrate during substrate rotation in setup 1.

The fragmentation degree at the four spray distances has been mapped out in terms of Re and MI (Fig. 8). The variation of average Reynolds number is about 100 from 60 to 120 mm in setup 2. With this Re range, a lower degree of fragmentation occurs at the 80 and 100 mm positions where the melting indices are relatively high, which indicates a larger fraction of fully melted particles. Accordingly, the splat images are mapped out as illustrated in Fig. 9. The morphology of splats out of this ex-

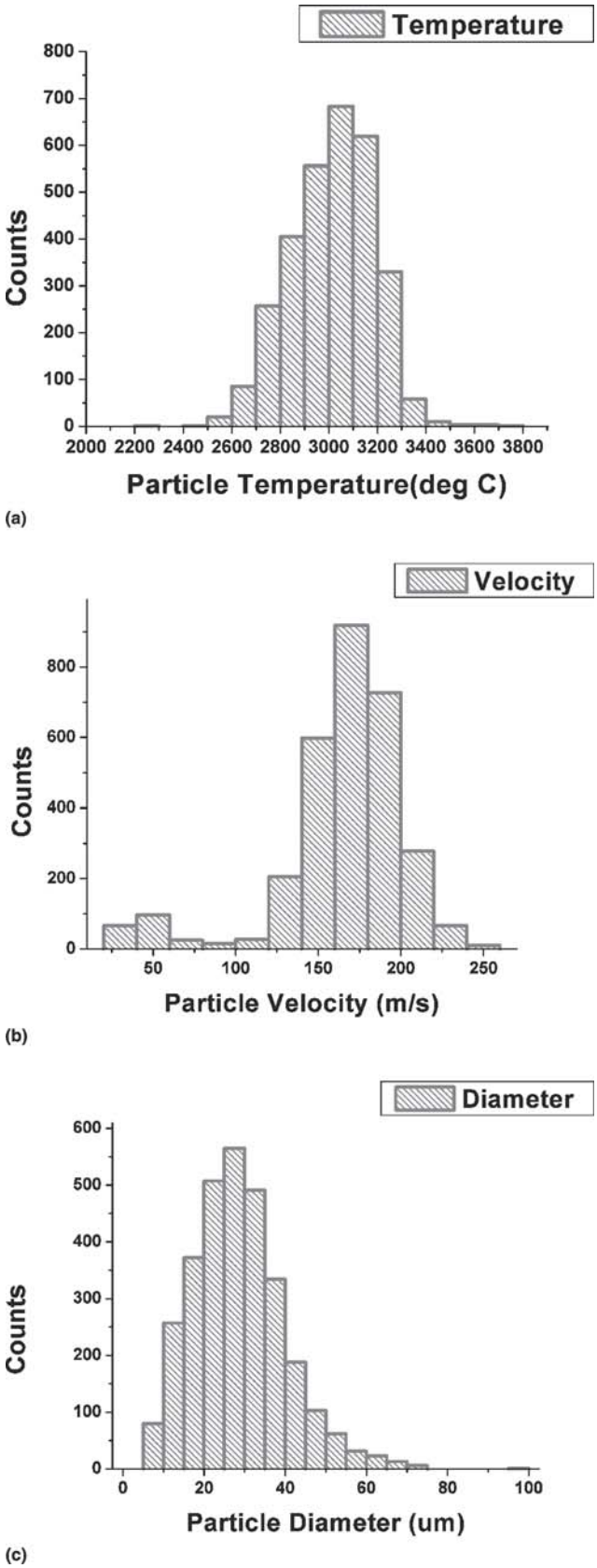

Fig. 3 Histograms of (a) in-flight particle temperature, (b) in-flight particle size, and (c) in-flight particle velocity

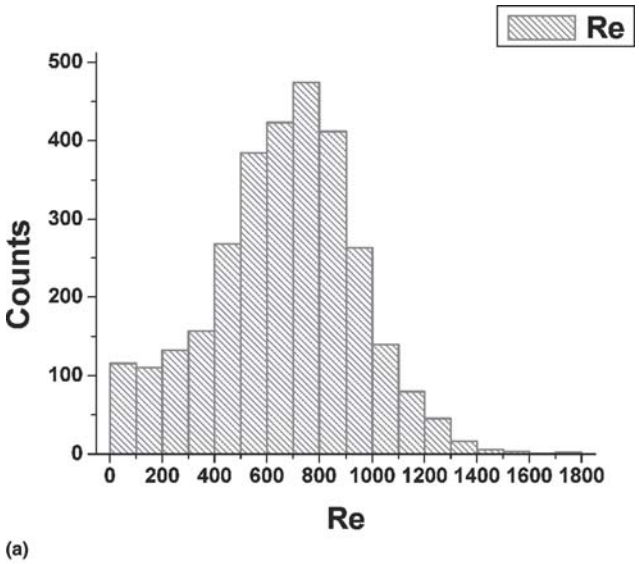

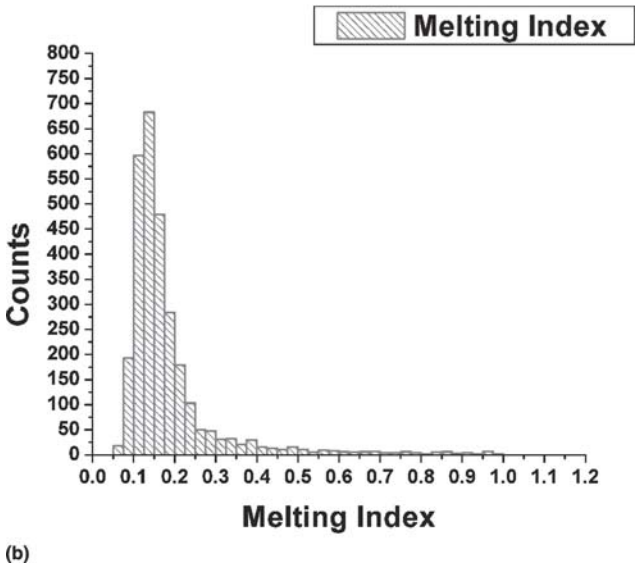

Fig. 4 Histograms of (a) particle *Re* and (b) particle *MI*

periment can be separated into three regions in accordance with particle *Re* and *MI*, i.e., limited fragmentation, unmelted and fragmented, and molten and fragmented.

4.3 Approaching Optimized Spray Distance

Figure 10(a) sketches the typical sample coupons after spraying in setup 2. Because the coupon size is larger than the flame size, all particles from the flame have the potential to be deposited on the substrate, and the width of deposit increases along the spray axis due to the conical shape of the particle trajectories (Fig. 10b). The deposition rate is plotted along the spray distance against average temperature, velocity, and *MI* (Fig. 11). The fact that only the *MI* curve matches the evolution of the deposition rate suggests that particle temperature and velocity cannot give a complete description of the in-flight particle state, so it is difficult to deduce the coating behavior accurately based only on

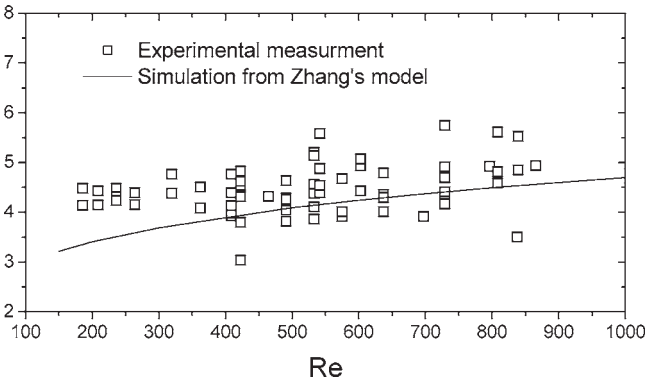

Fig. 5 Effect of *Re* on splat flattening ratio

them, whereas *MI* describes the particle quite well and agrees with the deposition properties in this case.

Because the *MI* can be used as an indicator for the deposition rate, an optimized target position, in terms of deposition rate, can be determined to be the position with the maximum *MI* value.

Therefore, at the optimized target position, the following equation should be satisfied:

$$\frac{\mathrm{d}(MI)}{\mathrm{d}L} = 0 \qquad \text{(Eq 2)}$$

For Bi $\ll$ 1, from Eq 1:

$$MI \propto \frac{\Delta T \cdot L}{d \cdot v} \qquad \text{(Eq 3)}$$

where

$$\Delta T = T_\mathrm{s} - T_\mathrm{m}$$

Assuming the particle velocity remains almost constant after acceleration in the core of the plasma jet:

$$\frac{\mathrm{d}(\Delta T \cdot L)}{\mathrm{d}L} = \frac{\mathrm{d}T_\mathrm{s}}{\mathrm{d}L} \cdot L + \Delta T = 0 \qquad \text{(Eq 4)}$$

and

$$\frac{\mathrm{d}T_\mathrm{s}}{\mathrm{d}L} \cdot L + \Delta T = \frac{\mathrm{d}T_\mathrm{s}}{\mathrm{d}t} \cdot \frac{\mathrm{d}t}{\mathrm{d}L} \cdot L + \Delta T = \frac{\mathrm{d}T_\mathrm{s}}{\mathrm{d}t} \cdot \frac{L}{v} + \Delta T = 0 \qquad \text{(Eq 5)}$$

Assuming spherical droplet, from energy balance:

$$-mC_\mathrm{p} \frac{\mathrm{d}T_\mathrm{s}}{\mathrm{d}t} = h\pi d^2 (T_\mathrm{s} - T_\mathrm{g}) \qquad \text{(Eq 6)}$$

where m is the mass of the droplet and C_p is the specific heat of the droplet. T_g is the surrounding gas temperature near the substrate.

Substituting Eq 6 into Eq 5 gives:

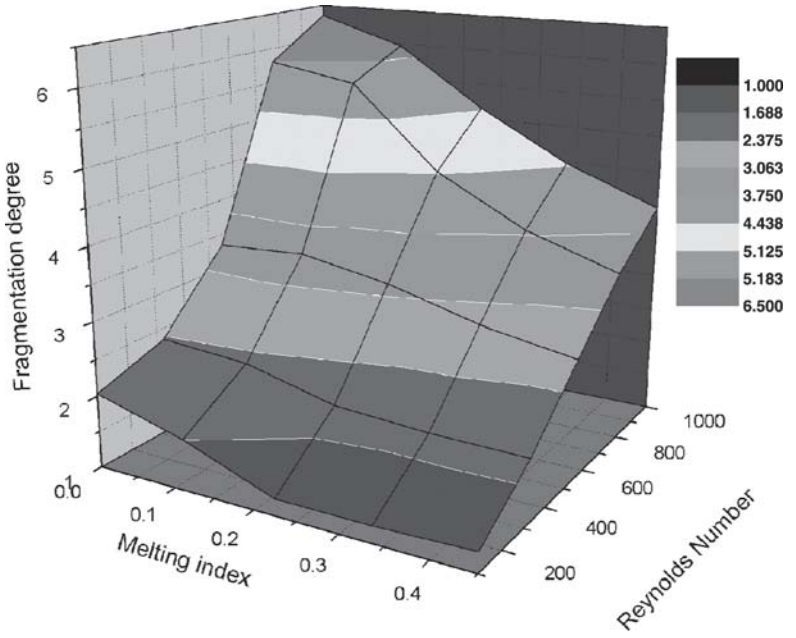

Fig. 6 Correlations between splat fragmentation degree and process parameters

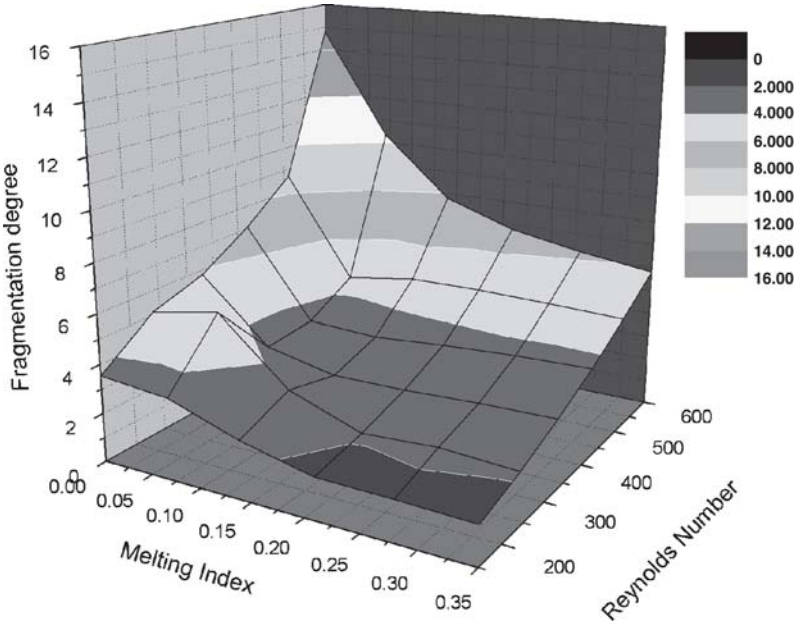

Fig. 7 Three dimensional map of splat fragmentation degree from setup 2

$$-\frac{h\pi d^2(T_s - T_g)}{mC_p}\cdot\frac{L}{v} + \Delta T = 0 \qquad \text{(Eq 7)}$$

Thus the optimized target position L_{opt} is:

$$L_{opt} = \frac{vmC_p(T_s - T_m)}{h\pi d^2(T_s - T_g)} = \frac{\rho C_p}{6h}\frac{vd(T_s - T_m)}{T_s - T_g} \qquad \text{(Eq 8)}$$

Although it is not currently possible to resolve the optimized target position L_{opt} for the experimental case using the equation above because h and T_g are could not be obtained precisely by the authors, Eq 8 does suggest the roles of particle parameters in determining the optimized spray distance. In general, particles with larger size and faster speed and experiencing lower heat transfer coefficient or lower heat input from ambience would need longer dwelling time to be fully melted. Accordingly, the substrate should be put in a certain distance from the torch, neither too close to ensure required dwelling time nor too far away to avoid particle cooling down in the plume. The results in this

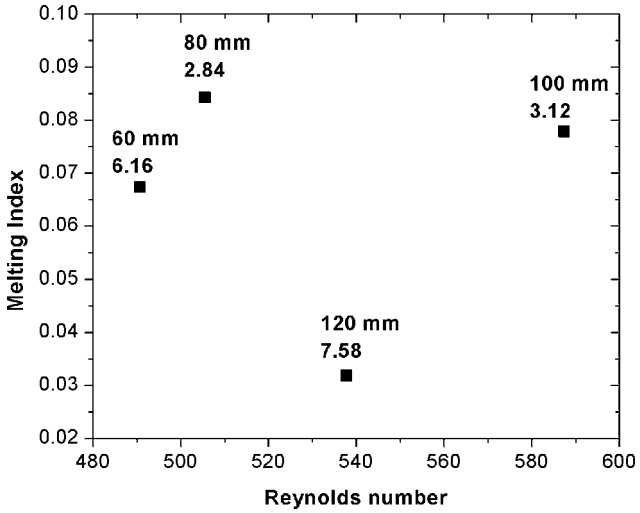

Fig. 8 Process parameters along spray distances and the consequent splat fragmentation degree

study indicate that the deposition rate is more closely correlated to the melting fraction of the particles upon impact. Thus, *MI* can be used as a control parameter to improve the spray yield. The possible correlations between deposition rate with *MI* is that fully melting particles of a large amount can reduce the fraction of bounce off of unmelted solid parts and improve the deposition rate. However, superheating the particle to a certain high temperature may encourage the vaporization of materials so that the deposition rate is reduced. Thus the superheating should be controlled to a certain extent to just improve the melting.

It is worth noting that two special cases, where $T_s = T_m$ and $T_s = T_g$, are certainly the limitations of Eq 8. The model derived here is to group analyze the in-flight particles with measurable parameters instead of physically describing individual droplet status. In practice, $T_s = T_m$ is a case in which most particles are under partially melted or unmelted conditions, which is to be avoided during the spraying process, whereas $T_s = T_g$ describes an equilibrium status between particles and surrounding gases, which is usually not the case in normal spraying conditions. A

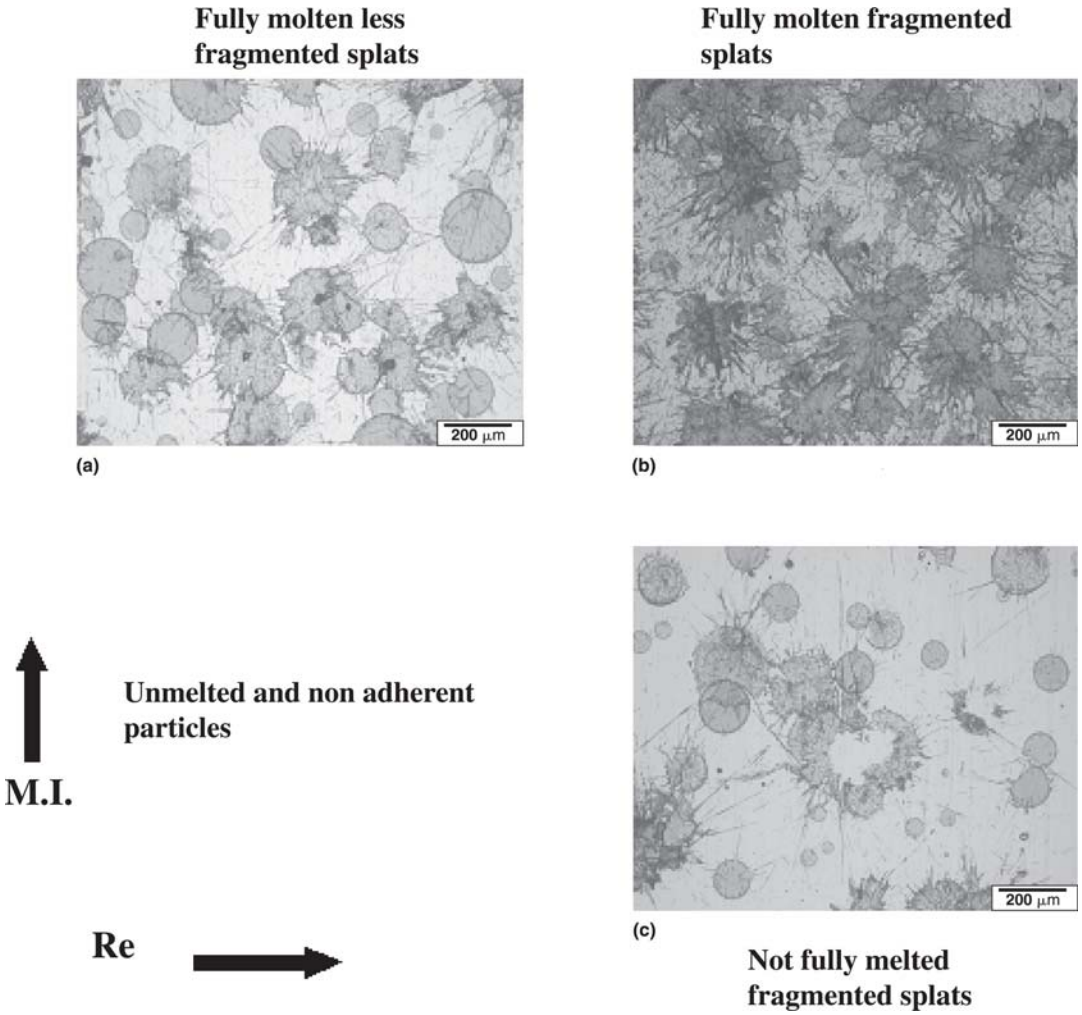

Fig. 9 Splat morphology interpreted by *Re* and *MI*: (a) splats from 80 mm spray distance, (b) splats from 60 mm spray distance, and (c) splats from 120 mm spray distance

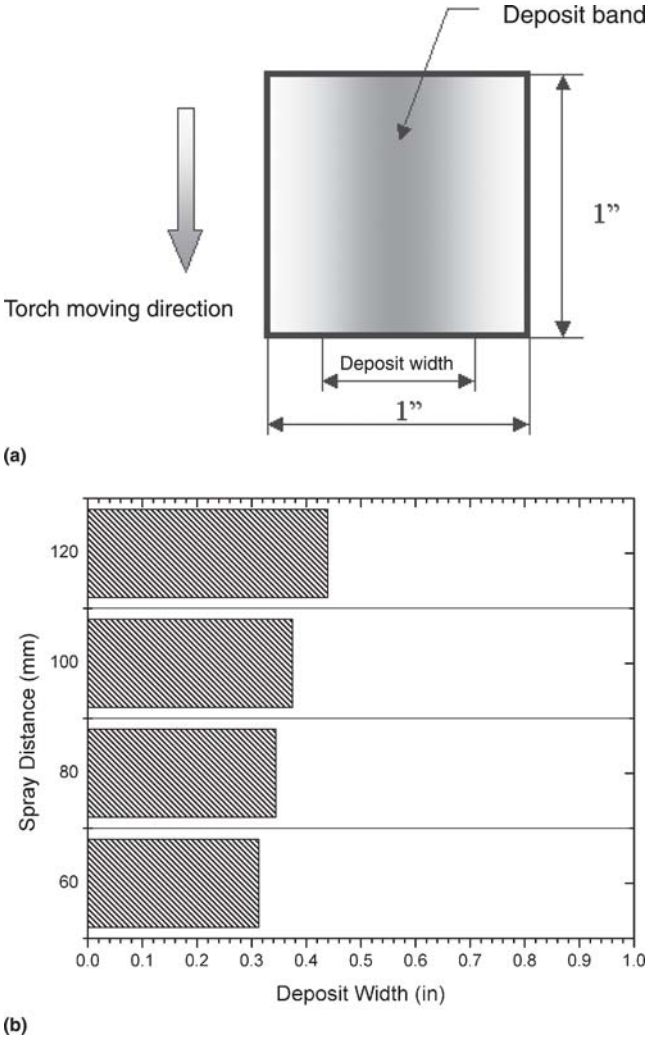

Fig. 10 (a) Sketch of the sample coupon after spraying and (b) deposit width along spray distance

refined model is to be developed to make up for these limitations.

5. Conclusions

Thermally sprayed partially stabilized zirconia particles and the splats formed after impact have been systematically investigated in this study. It was found that the deposition rate is dependent upon the melting fraction of the particles. The correlation between the group parameters, *Re*, and *MI*, and the splat flattening behavior reveals that the particle's kinetic energy and its molten status are critical in determining the splat morphology. For zirconia particles, full melting requires a large value of *MI*. Particles tend to fragment at high *Re*; however the fragmentation mechanism is different at high and low melting status. In summary, the morphology of splats can be roughly separated into three regions: limited fragmentation, unmelted and fragmented, as well as molten and fragmented. Accordingly, the optimized spray distance in terms of deposition rate can be assumed at the apex of the *MI* curve.

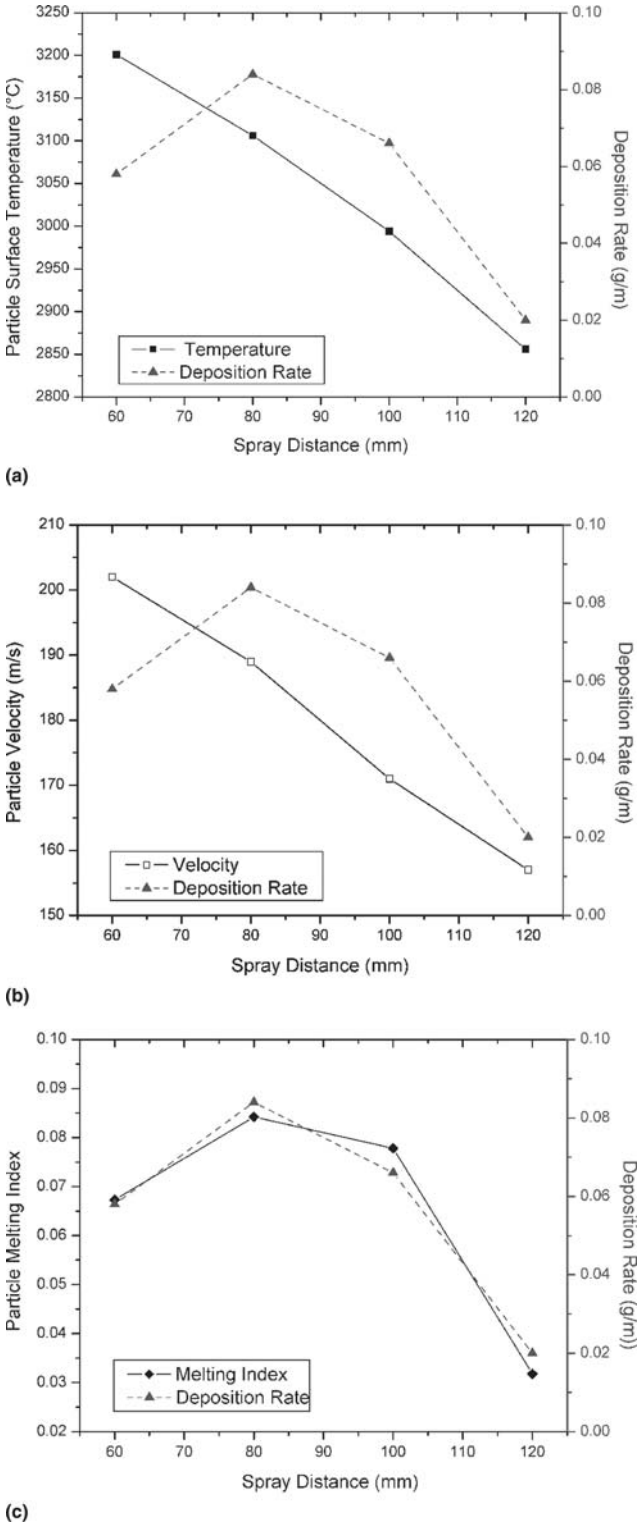

Fig. 11 Correlations of deposition rate and particle in-flight parameters: (a) surface temperature, (b) velocity, and (c) *MI*

Acknowledgments

The authors thank Glenn Bancke for the help in spraying and Prof. Hui Zhang and Dr.Tilo Streibl for stimulating discussion and contributions. This work was supported by the MRSEC pro-

gram of the National Science Foundation under Award No. DMR-0080021.

References

1. S. Fantassi, M. Vardelle, A. Vardelle, and P. Fauchais, Influence of the Velocity of Plasma-sprayed Particles on Splat Formation, *J. Therm. Spray Technol.,* 1993, 2 (4), p 379-384
2. M. Vardelle, A. Vardelle, A.C. Leger, P. Fauchais, and D. Gobin, Influence of Particle Parameters at Impact on Splat Formation and Solidification in Plasma Spraying Processes, *J. Therm. Spray Technol.,* 1995, 4 (1), p 50-58
3. R.N. Wright, J.R. Fincke, W.D. Swank, and D.C. Haggard, Particle Velocity and Temperature Influences on Microstructure of Plasma Sprayed Nickel, *Thermal Spray: Practical Solution For Engineering Problems,* C.C. Berndt, Ed., Cincinnati, OH, ASM International, 1996, p 511-516
4. X.Y. Jiang, "Deposit Formation Dynamics and Microstructure Development during Thermal Spraying," Ph.D. dissertation, State University of New York at Stony Brook, Stony Brook, NY, 2000
5. M. Friis, C. Persson, and J. Wigren, Influence of Particle In-Flight characteristics on the Microstructure of Atmospheric Plasma Sprayed Yttria Stabilized ZrO_2, *Surf. Coat. Technol.,* 2001, 141 (2-3), p 115-127
6. M. Prystay, P. Gougeon, and C. Moreau, Structure of Plasma-Sprayed Zirconia Coatings Tailored by Controlling the Temperature and Velocity of the Sprayed Particles, *J. Therm. Spray Technol.,* 2001, 10 (1), p 67-75
7. J. Madejski, Solidification of Droplets on A Cold Surface, *Int. J. Heat Mass Transfer,* 1976, 19, p 1009-1013
8. H. Zhang, Theoretical Analysis of Spreading and Solidification of Molten Droplet During Thermal Spray Deposition, *Int. J. Heat Mass Transfer,* 1999, 42, p 2499-2508
9. D. Bergmann, U. Fritsching, and K. Bauckhage, A Mathematical Model for Cooling and Rapid Solidification of Molten Metal Droplets, *Int. J. Therm. Sci.,* 2000, 39 (1), p 53-62
10. Y.P. Wan, V. Prasad, G.X. Wang, S. Sampath, and J.R. Fincke, Model and Powder Particle Heating, Melting, Resolidification, and Evaporation in Plasma Spraying Processes, *J. Heat Transfer-Trans. ASME,* 1999, 121 (3), p 691-699
11. Y.P. Wan, J.R. Fincke, S. Sampath, V. Prasad, and H. Herman, Modeling and Experimental Observation of Evaporation from Oxidizing Molybdenum Particles Entrained in a Thermal Plasma Jet, *Int. J. Heat Mass Trans.,* 2002, 45 (5), p 1007-1015
12. A. Vaidya, G. Bancke, S. Sampath, and H. Herman, Influence of Process Variables on the Plasma Sprayed Coatings, *Thermal Spray 2001: New Surfaces For A New Millennium*. C.C. Berndt, K.A. Khor, and E. Lugscheider, Ed., Singapore, ASM International, 2001, p 1345-1349
13. H. Zhang, H.B. Xiong, L.L. Zheng, A. Vaidya, and L. Li, Partially Melted Particle and Its Splat Morphology, in *Thermal Spray 2003: Advancing the Science & Applying the Technology,* C. Moreau, Ed., Orlando, FL, ASM International, 2003, p 905-911
14. C. Moreau, M. Lamontagne, and P. Cielo, U.S. Patent 5, 180, 921, Nov, 1991
15. P. Degroot and L. Deck, Surface Profiling by Analysis of White-Light Interferograms in the Spatial-Frequency Domain, *J. Mod. Opt.,* 1995, 42 (2), p 389-401
16. J.C. Davis, *Statistics and Data Analysis in Geology,* John Wiley & Sons, New York, 1986
17. C.J. Li, J.-L. Li, and W-B. Wang, The Effect of Substrate Preheating and Surface Organic Covering on Splat Formation, *Thermal Spray: Meeting the Challenges of the 21st century,* C. Coddet, Ed., Nice, France, ASM International, 1998, p 473-480
18. Y. Tanaka and M. Fukumoto, Investigation of dominating factors on flattening behavior of plasma sprayed ceramic particles, *Surf. Coat. Technol.,* 1999, 121, p 124-130
19. X.Y. Jiang, Y.P. Wan, H. Herman, and S. Sampath, Role of condensates and adsorbates on substrate surface on fragmentation of impinging molten droplets during thermal spray, *Thin Solid Films,* 2001, 385 (1-2), p 132-141